PROCEEDINGS REPRINT

SPIE—The International Society for Optical Engineering

Reprinted from

Space Processing of Materials

4–5 August 1996
Denver, Colorado

Volume 2809

Advancement of x-ray microscopy technology and it's application to metal solidification studies

William F. Kaukler
CMMR, The University of Alabama in Huntsville, Huntsville AL 35899

Peter A. Curreri
NASA, Marshal Space Flight Center, ES75, MSFC AL 35812

Keywords: x-ray, microscope, solidification, microfocus, real-time, scintillator, CCD, MTF, EBCCD, CsI

ABSTRACT

The technique of x-ray projection microscopy is being used to view, in real time, the structures and dynamics of the solid-liquid interface during solidification. By employing a hard x-ray source with sub-micron dimensions, resolutions of 2 μm can be obtained with magnifications of over 800 X.

Specimen growth conditions need to be optimized and the best imaging technologies applied to maintain x-ray image resolution, contrast and sensitivity. It turns out that no single imaging technology offers the best solution and traditional methods like radiographic film cannot be used due to specimen motion (solidification). In addition, a special furnace design is required to permit controlled growth conditions and still offer maximum resolution and image contrast.

INTRODUCTION

The objective of this work was to develop an advanced x-ray microscope for studying fundamental solidification dynamics of opaque metal alloys and semiconductors. Real-time x-ray microscopy with sufficient resolution of solidifying solid/liquid interfaces can provide unambiguous testing of current alloy solidification models[1] by providing precise data of the shape and extent of the solute boundary layer, real growth rate, solid liquid interfacial morphology, as well as the nucleation, coalescence, and incorporation into the solid of the phases. Further, we believe that there could be substantial benefit in the employment of a high resolution x-ray microscope for solidification studies in space. It will enable efficient testing of hypotheses to explain the eutectic phase spacing changes in microgravity, allow quantitative monitoring of interface shape differences and measure concentration gradients in the solute boundary layer in microgravity. Thus, a secondary object of this work is to focus on hardware options that have potential for development into a microgravity materials science flight apparatus for possible implementation on a Space Station furnace.

With current technology, the most directly applicable x-ray microscopy method for the study metal solidification in-situ is x-ray transmission or projection microscopy (XTM) which relies on the differential adsorption of the x-ray beam to provide contrast and thus has potential to the image concentration gradients in the liquid. There are four other real-time x-ray microscopy methodologies: a) X-ray topography, in which contrast is obtained from complex diffraction phenomena in crystals. Synchrotron beams are the most suitable. Exposures on film take seconds but can be examined with optical magnification, but real-time capability is available. b) Imaging x-ray optics are being developed using grazing incidence mirrors, zone plates (diffraction lenses) or multi-layer optics (diffraction mirrors) since x-rays cannot be refracted by lenses.[2] However, all such systems presently employ very soft x-rays which are not suited to metal specimens. c) Scanning X-ray microscopes utilizing Fresnel zone plate focusing have achieved resolutions of 0.25 μm imaging biological specimens but require a coherent soft X-ray beam only available by utilizing a major synchrotron radiation facility. Scanning rates are too slow to follow solidification dynamics.[2] d) X-ray Microtomography is like conventional (CAT) tomography but can offer down to 1 μm resolution. Real-time studies are not currently feasible since it takes 20 minutes or more to for a scan at the higher resolutions.

Radiography of liquid metal has been utilized with sources allowing resolution 300 to 500 μm which have been used effectively to image shrinkage porosity[3], melt solid interface shape[4], and the convection caused by dissolving wires.[5] However, the imaging of the many critical microstructural features require resolution of 1-100 μm. A X-ray source

0-8194-2197-9/96/$6.00

capable of this resolution, but with less flux than optimal for metals has been used[6] to determine the concentration gradients of zinc ions in aqueous solutions. Dendrites and channel formation in aluminum alloys were studied[7-8] utilizing film for resolutions up to 10 micrometers and real-time data with an X-ray vidicon camera with video tape with resolutions of about 100 micrometers. Although the vidicon, which is a charge induction type detector, can produce reasonable resolution, it has poor sensitivity at lower photon flux levels[9] thus limiting its dynamic range. With state-of-the-art x-ray image converters and cameras, the 2-3% difference in x-ray absorption between crystalline and liquid aluminum provides sufficient contrast to observe this interface. Imaging of metal solid-liquid interfaces in real-time with x-rays requires performance near the limit of technological feasibility.

In this paper we report the performance of an XTM utilizing a state of the art sub-micron source, capable of 10 to 100 keV acceleration energies, x-ray image tube intensifier, and cooled charge coupled device (CCD) detector, to image the directional solidification of metal alloys in real time (10 second frame rate) with resolutions of up to 30 μm. With this apparatus we have successfully imaged in real time for solidifying metal alloys, interfacial morphologies, real growth rate, nucleation, coalescence, incorporation of phases into the growing interface, and the solute boundary layer in the liquid. We will then discuss our current efforts to increase real-time resolution by improved furnace design, and by more advanced camera/converter technologies.

EXPERIMENTAL METHODS

Figure 1 is a schematic diagram showing the XTM being applied to image a specimen in a relatively x-ray transparent crucible. A divergent beam of x-rays is generated at the (sub-micron sized) focus of an accelerated beam of electrons where they interact with a thin tungsten film supported on a beryllium substrate. Magnified images are produced by projection where the source spot size essentially determines the limit to resolution of the images. Since there are no 'optics', there is no focusing of the image and they have *infinite* depth of field. The x-ray shadow (image) of the specimen is converted to a digital image for display and study. The specimen crucible is positioned in a horizontal gradient furnace design similar to a Bridgman crystal growth system. The sample dimension is 50 x 20 mm and 1 mm thick in the x-ray transmission direction. It is completely enclosed in a flat boron nitride crucible to retain its shape during melting. The furnace housing is water cooled. The minimum specimen distance from the focal spot of the source is at least 11 mm. Aluminum foil windows prevent excessive heat losses from the sample with a small attenuation of the x-ray flux. Using a single-zone heater arrangement, the temperature gradient is typically from 44 to 52 °C/cm in the vicinity of the interface. The specimen and crucible are pulled at a controlled rate through this gradient. This

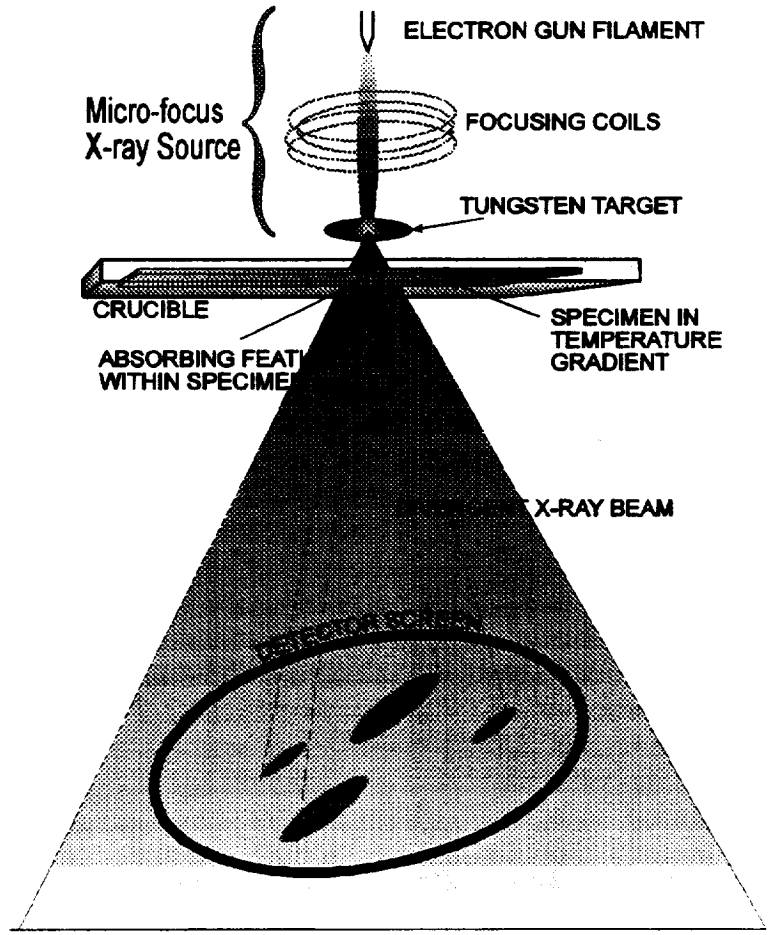

Figure 1. X-ray Transmission Microscope for solidification studies schematic diagram showing image projection from micro-focus source.

arrangement maintains the solid-liquid interface within the field of the microscope for continuous viewing. A DC motor-driven screw pushes/pulls the specimen in its crucible at rates of 1 to 20 μm/sec normal to the x-ray beam.

Specimens having the above dimensions were prepared from castings of pure Al or Al alloys prepared using 5 N purity components (Ag, Cu, Pb, or In). Castings were made both in air and argon with graphite crucibles.

RESULTS

Understanding the formation and selection of morphologies during the breakdown of the planar solid/liquid to the cellular structures caused by constitutional undercooling is of considerable importance to metallurgy. Most previous studies have relied on the use of transparent organic or salt models.[10-12] But the phase structure of these systems are often simplified and their thermophysical and transport properties differ significantly from metallic systems. Thus the XTM fills a fundamental need for an experimental technique that can monitor these parameters precisely, in real time during the morphological instability of opaque metal systems. The onset of the instability can, utilizing the XTM, be observed in real-time.[13] See Fig. 2, right side. Planar interfaces are ordinary in appearance but occasionally, under the XTM, interesting features like grain boundaries that intersect the solid-liquid interface can be found (Fig. 2, left side). (Losses incurred through printing the images obscure the darker band of solute found in the liquid against the solid in these Al-Ag alloys.) However, the solute boundary layer is clearly seen in the monotectic

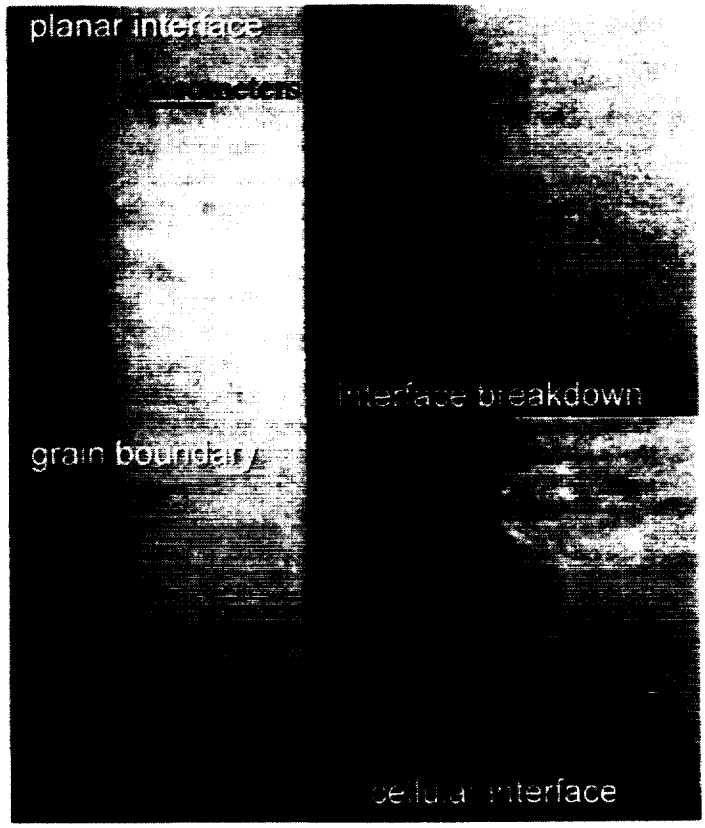

Figure 2. Al 2% Ag interfaces.[13] Each are 2 second exposures at 55 kV acceleration and 200 μA current. Left figure shows planar interface growing at 1 μm/sec; grain boundaries intersect the interface isotherm. Upper right image captured the initial stages of cellular breakdown after the rate was increased to 2 μm/sec from 1.5 μm/sec. The lower right part shows the steady state cellular growth at 2 μm/sec.

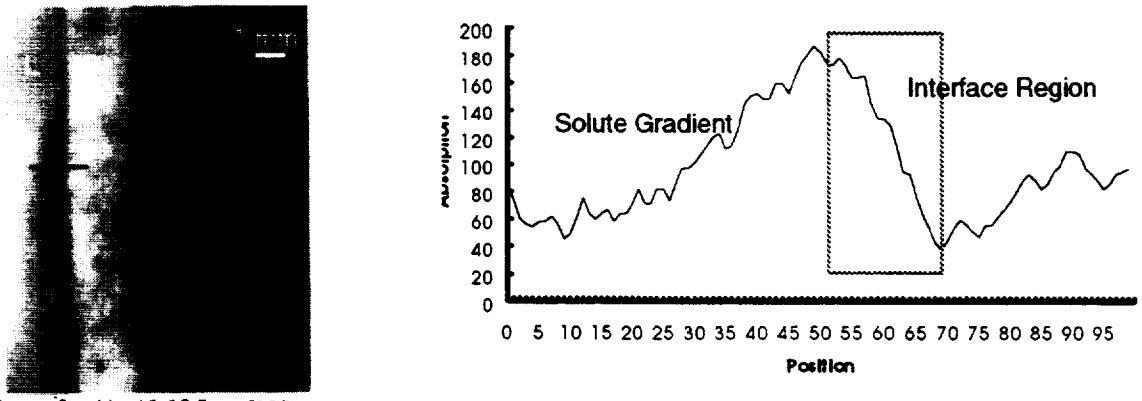

Figure 3. A) Al-18 In solid/liquid interface growing at 12.4 μm/sec in a 45 °C/cm temperature gradient showing solute rejection to the liquid after the step increase of translation rate. B) Optical intensity (absorption) profile along the line in A) crossing the solute layer and interface. Solute gradient is clearly seen on the left part of the graph. Increasing In content represents increased absorption. The diffuse interface region is in the marked area. Note the solute layer is not uniform along the length of the interface.

alloys we have studied[14-15] when the growth rate was sufficiently high (Figure 3). The right part of the figure shows the optical density (absorption) profile along the line shown crossing the interface and the solute layer in the liquid. Planar interfaces become a baseline structure for measurements of the perturbation of the interface shape when nearby a void or particle. Figure 4 shows the interface distortions caused by two voids that formed as a result of the coalescence of rejected gas impurities during solidification. Some of these voids become engulfed by the solid and attain an elongated shape.

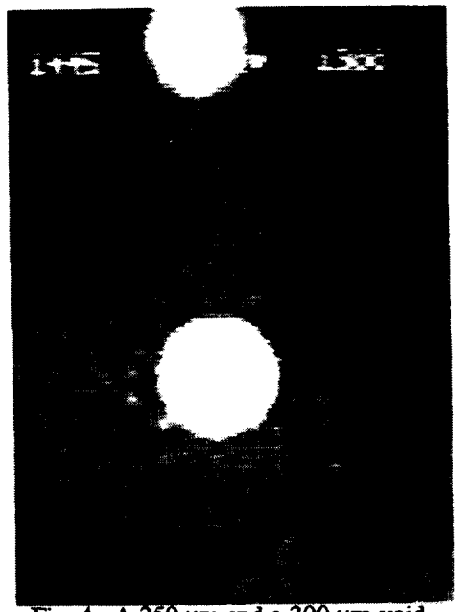

Fig. 4. A 250 μm and a 300 μm void in Al at a solid-liquid interface showing the local curvature caused by the low thermal conductivity of the voids. The interface is growing from right to left at 2 μm/sec in a 45 °C/cm temperature gradient.

DISCUSSION

The XTM utilizing a state of the art sub-micron source, x-ray image tube intensifier, and cooled charge coupled device (CCD) camera, is capable, as is demonstrated by the above results, of imaging the directional solidification of metal alloys in real-time (10 second frame rate) with resolutions of up to 30 μm. This capability provides a valuable tool for the study of the solidification dynamics in metal alloys and semiconductor materials. However, for the study of the dynamics of formation of some important features, such as eutectic or monotectic fibers, a real-time resolution of 1-10 μm is required. Our current efforts to increase real-time resolution concentrates on two approaches - improved furnace design, and more advanced camera/converter technologies.

Advanced Furnace Development

The furnace design and XTM configuration described above provided a maximum magnification about 35 X. The magnification, M, at the image detector (converter) screen is given by $M = (a+b)/a$, where a is the distance form the source to the sample, and b is the distance from the sample to the converter. This was illustrated in Fig. 1. For specimens very close to the source we can obtain magnification of over 800 X. When the magnification is not limited by the furnace housing, we can achieve a resolution of up to 2 μm. Figure 5 shows the fibrous structures in the Al-Pb monotectic (which are about 5 μm diameter) when imaged post solidification. These fibers could not be resolved during solidification due to the magnification limit imposed by the furnace and image intensifier tube.

Thus one approach to be able to view the formation of fine structures like eutectic fibers and dendrites in-situ is to design a furnace that can safely bring a 1200° C heating element within a few millimeters of the room temperature source. We were unable to find insulation that adequately protects the x-ray source with this spacing. Instead we are developing a furnace design that uses flowing, chilled water to protect the outside of the furnace. Both thermal radiation and conduction are significant modes of heat transport in this temperature range so some thin

Figure 5. Post-solidification high magnification radiomicrograph of Al-1.5 Pb monotectic alloy showing fine fibers of Pb. This specimen was unidirectionally grown at 1 μm/sec in a temperature gradient of 45 °C/cm. The fibers can be seen to grow somewhat aligned on the left and meandering or twisting on the right due to some unknown phenomenon.

insulation was also required between the heater and the furnace wall. The upper, critical surface of the furnace is one millimeter thick and made from a copper alloy foil water jacket. The remainder of the gap between the specimen crucible and the outside of the furnace is a high-alumina fibrous ceramic insulation capable of withstanding continuous contact to the heating element in air. A cross-section view of the advanced furnace is shown in Fig. 6. The furnace is currently being tested. The advantage of this approach is that it could yield higher resolution without needing to increase the performance of the camera / converter system. One disadvantage is that when the specimen is placed very close to the x-ray source, due to the steep magnification vs. position relation, a moderate difference (< 10%) in magnification through the 1 mm sample thickness appears in the image.

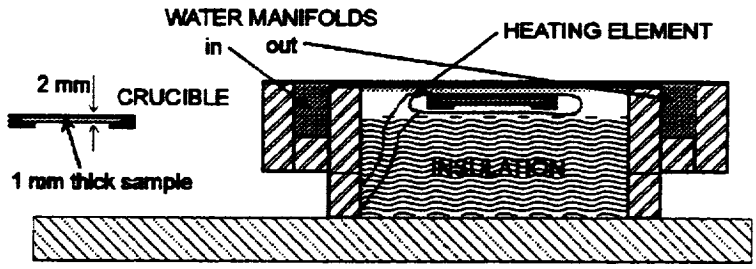

Figure 6. Cross section schematic of x-ray furnace and of sample in crucible.

Lower growth rates are desirable to allow adjustment of some feature dimensions through control of solidification kinetics. To provide these low rates (0.005 μm/sec minimum) and still provide relatively high rates (10,000 μm/sec maximum), a 100,000 step per revolution stepper motor was chosen. Computer control of the stepper motor offers significant additional benefits such as knowledge of position, the ability to repeat growth sequences, and the ability to vary the rate during growth according to a program.

Advanced x-ray image conversion/detection system

The primary limit to the real-time resolution of the solidification XTM is the device to convert the x-ray shadow into usable images. Five technologies, all using CCDs, were evaluated for this. Some of these technologies are several years old and others, state of the art. The oldest technology (invented 1950s) is the x-ray image intensifier tube. We used the state of the art (1990) tube technology (Thompson CSF, 9 inch tri-field tube, model TH 9428 HP). However, with this technology, signal gain is traded for resolution. The intensifier tube coupled with a cooled (12 bit) CCD camera (Photometrics Series 200 with full frame Kodak 1100x1300 sensor) yielded the real time images shown in the above figures. The image quality of these experiments was limited by this intensifier tube technology. This is readily seen when comparing the MTF* curves shown in Fig. 7 and the resolution data in Table 1. (Two other curves in Fig. 7 are for CCD sensors and will be discussed later). The limiting resolution of this intensifier tube is 125 μm. Since smaller features cannot be resolved well with the this intensifier tube, magnification of the x-ray image is needed to resolve microscopic features and move up on the MTF curve. This is most apparent when we attempt to observe the finest microstructures. This tube and housing (includes shielding) is about one cubic foot in size and is quite heavy. Although there are other, more compact designs, it is still unattractive for use in a space flight apparatus.

CCD technology is well established. CCDs have a very high detection efficiency (DQE or detector quantum efficiency) with visible light wavelengths. Much recent progress in the imaging of hard x-rays[16] has been made by utilizing the rapidly advancing CCD solid state image detector technology. The CCD can be used for direct imaging of the x-ray radiation (above 1 keV). They provide the numerous benefits for digital image processing and offer real-time tracking of dynamic processes (such as solidification phenomena). The issues of contrast, resolution, signal to noise ratio, and sensitivity must simultaneously be examined.

* MTF Modulation Transfer Function, a measure of the loss of resolution and contrast due to the passage of a signal (image) through a signal processing device. The function relates the outgoing signal (amplitude range) to the incoming as a function of the signal's frequency (eg. line pairs per mm on the image). The smaller the features, the greater the signal loss - always. Imagine: an x-ray image starts with less than 100% contrast, like the 3% contrast of a s/l Al interface. After conversion to a digital image, the output contrast could be much less than 3%.

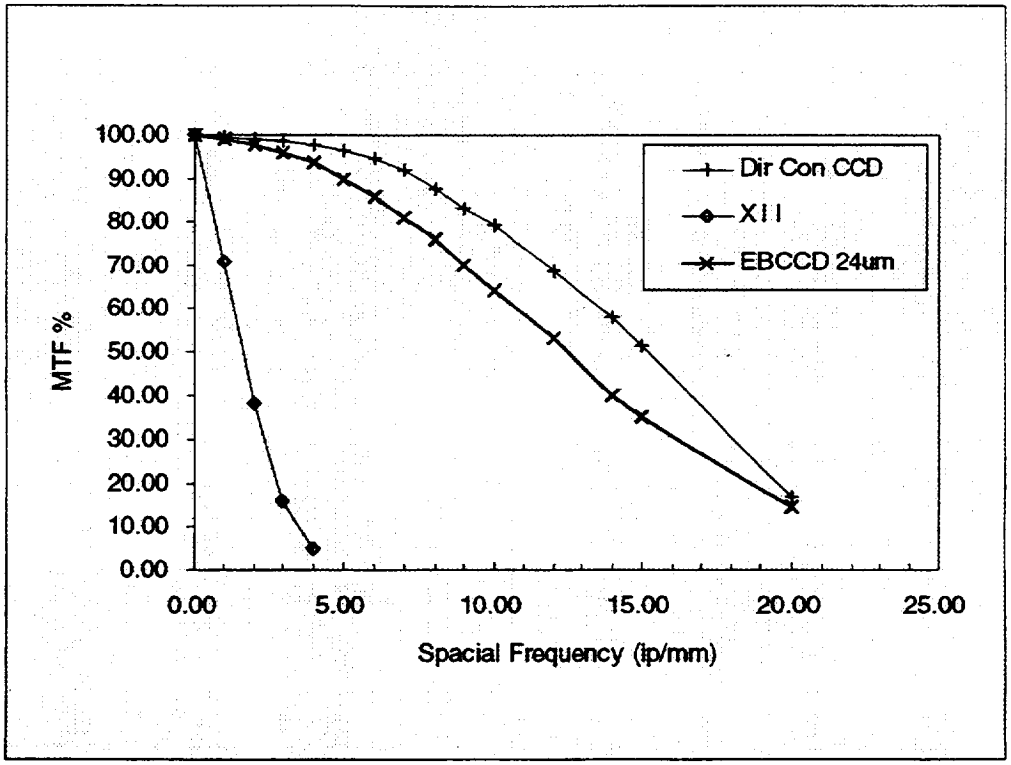

Figure 7. The graph compares the manufacturer's MTF of the Thompson CSF TH9428 HP x-ray image intensifier (XII) tube[21] to the measured MTF of a 25 μm pixel size direct conversion x-ray CCD[18] (with 8 keV photons) and of the electron bombarded CCD (EBCCD) device[19] of Fig. 6 (in visible light) using a back-thinned SITe SI502AB CCD having 24 μm pixels.

Table I: comparison of converter/camera properties:

#	Description	Max. Resolution lp/mm	lp/mm @ 50% MTF	X-ray DQE
1	Thompson CSF 9" X-ray intensifier tube (TH9428HP) [21]	4	1.4	65%
2	CsI on CCD[a]	17	?	min 20%[22]
3	CsI on FO on CCD[a]	22+	?	min 25%[22]
4	Direct Conversion CCD	22+[a]	15[18]	10% @ 10 keV, 2% @ 35 keV[22]
5	Pixel Vision EBCCD[19]	50	30	min 20%[a]
6	Radiographic film	>100[a]	?	4% @ 70 keV[17]

a based on measurements made in this work

Thus in order improve the real-time resolution of the XTM over that obtainable utilizing the intensifier tube technology we evaluated CCD based conversion systems. Fig. 8 shows the schematic diagrams for three evaluated. CCD sensors. From left to right are the direct conversion CCD, the scintillator deposited on the CCD and the scintillator deposited on a fiberoptic faceplate bonded to the CCD. Arriving from the top in each diagram, is shown an x-ray photon which is absorbed in the converter layer. These diagrams show the critical components of the sensors in a magnified, cross-sectional view. Figure 5 is the corresponding set of resolution test images from the sensors in Fig. 4. These images were obtained from engineering grade CCD sensors (having a few known faults but suited for evaluation purposes) from EEV in England. EEV offers all three versions of sensor with a large full-well per pixel capacity. Full-well electron

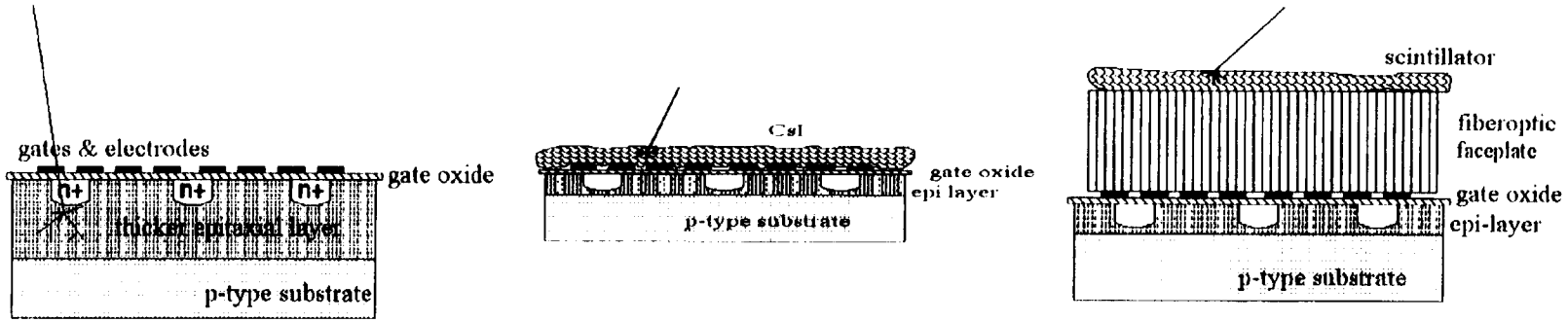

Figures 8. From left to right above: direct conversion CCD schematic, scintillator deposited on CCD schematic, scintillator on fiberoptic faceplate on CCD schematic.

Figure 9. From left to right below: images from sensors as shown above; direct conversion CCD with 50 µm 'epi' layer, 120 µm CsI phosphor deposit on CCD, 120 µm CsI phosphor deposit on fiberoptic faceplate bonded to CCD. These images were aproximately 0.1 second contact exposures of a standard line-pair gage with the source operating with 50 kV acceleration and 350 µA current 5 inches away.

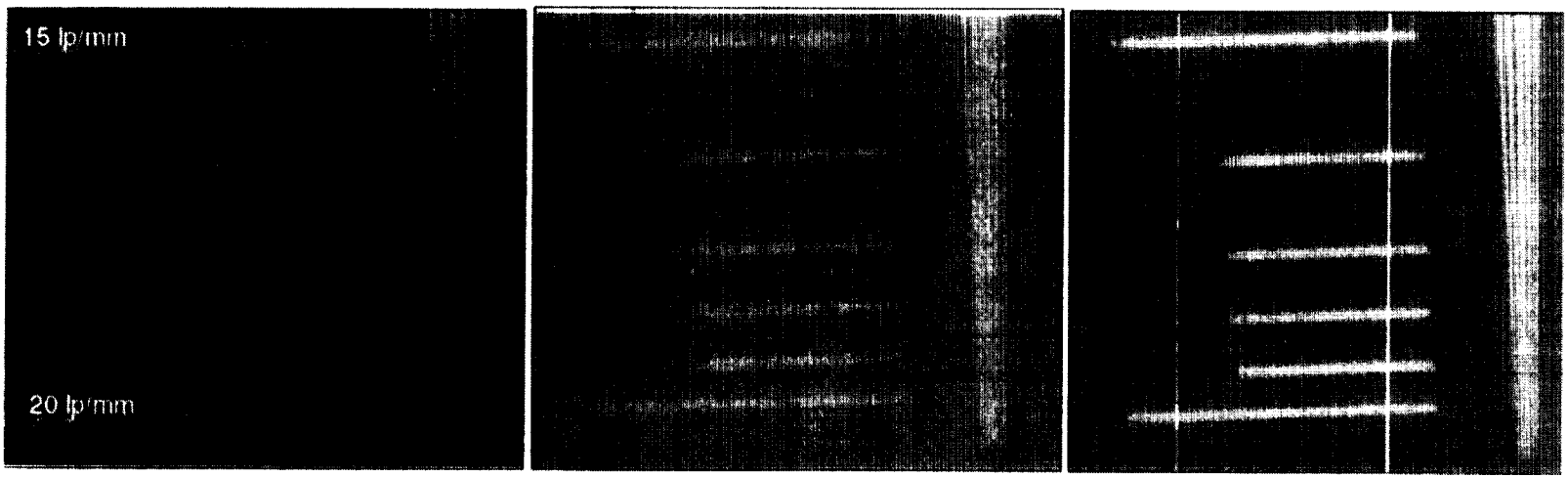

capacity of the pixel is set by its volume and is limited to about 500,000 for the devices we are interested in. Dynamic range of the sensor is in part limited by this well-depth. These were 0.85 x 1.2 cm devices (model CCD 02-06) with 578 x 385 pixels of 22 μm size. Cooling the CCD was not required for comparison proposes so, due to thermal noise, only 8-bit images were obtained. The images in the figure are contact radiographs using a commercial line-pair gage made from etched lead and can resolve 22 line-pairs per mm (lp/mm). Exposures were made at 50 kV acceleration and 350 μA current for the source with a duration of about 0.1 sec. The CCDs were 5 inches from the source and covered by one layer of Al foil.

Comparison of CCD x-ray sensors

In the direct conversion CCD (Fig. 8, left) x-rays are detected by absorption in the silicon of the CCD itself. X-ray hardened CCDs have only been practical in the last few years. Radiation damage accumulates although at a much slower rate than in conventional CCDs. The CCD would need replacement about every two years. Efficiency is favored at lower photon energies (<10 keV photons). Silicon has a low cross-section compared to the scintillator materials and so will not stop as many x-rays above these energies thus providing less signal. To compensate for this, the absorption (epitaxial or epi) layer was thickened from the typical 5 micrometers to 50 micrometers to capture more x-rays. The substrate is made from a high resistivity p-type Si. Still, less than 0.5% of 40 keV x-ray photons are absorbed in the sensor.[17] This method offers the best resolution since little scattering is incurred within the CCD (compared to thick phosphor coatings). The direct conversion CCD technology offers a high MTF. Figure 7 has a measured MTF of a direct conversion CCD sensor with 25 μm pixels.[18] This sensor is comparable to the one we evaluated. This curve shows over an order of magnitude improvement over the intensifier tube. The resolution of this device is also better than the scintillator based sensors as can be determined by comparing the images in Fig. 9.

The CsI coated CCD is shown in Fig. 8, center. This scintillator shields the CCD from x-rays. Thicker coatings can absorb more x-rays and both increase capture efficiency (DQE) and better protect the CCD. However, thicker coatings decrease image spatial resolution. High noise levels can occur if x-rays transmitted through the coating are absorbed by the silicon in the CCD since many ($> 10^4$) electrons will be created from each single photon captured and brighten that pixel. It's desired that all x-rays be totally absorbed in the scintillator layer which implies that all photons are converted.

A fiberoptic faceplate added to the CCD which is coated with CsI scintillator is shown in Fig. 8, right. A fiberoptic faceplate is a bundle of glass fibers fused together and cut normal to the bundle axis into a thin plate. Each fiber is a conduit of light on the 5-10 μm scale. The fiberoptic could also be tapered with a 2:1 or more ratio in front face diameter to rear face diameter. This latter arrangement has found use in x-ray crystallography and mammography applications. However, to reduce losses in the fiberoptic and because a large field of view is not required, the fiberoptic faceplate we employed is only 3 mm thick and has a 1:1 ratio. (A simpler approach would be to use a camera with a lens. However, far more light is lost this way.) We can permit a thinner phosphor coating on the fiberoptic because the x-rays passing through the layer will be absorbed by the glass faceplate before damaging the CCD or adding noise. Thinner coatings improve resolution by reducing scatter within the coating. Coupling losses (phosphor to CCD) are increased but spurious signals from stray x-rays getting into the CCD elements is eliminated.

The brightest image was obtained from the CsI coated CCD (as expected) while the direct conversion was the least bright for equivalent exposures. However, apparent resolution was not so good. Intuitively, the CsI on the CCD sensor should be superior, but the scintillator fills the gaps between the pixels and so reduces resolution by spilling light into adjacent pixels. The fiberoptic faceplate constrains the light from the scintillator into small bundles and directs it to the CCD pixels. Only glass fibers situated on a pixel element will illuminate it. The small loss of light is compensated by the improved resolution (Fig. 9) and protection of the CCD from x-rays. Research is presently under way to deposit the scintillator onto the pixels themselves but the best approach to date is still the fiberoptic faceplate.

Electron-bombarded CCD and other sensors

Recent developments in electron-bombarded CCDs (EBCCD) provide amplification necessary for night vision at video rates in a package comparable in size to a quarter.[19] The EBCCD technology has quantum noise limitation and

performance near theoretically optimum.[20] The EBCCD is available as a low light level imaging sensor. The visible light image is converted to an electron image by a photocathode deposit on a window in a vacuum tube. By impressing a high electric field between this photocathode and a nearby CCD, the electrons are accelerated into the CCD where they are collected (thus the name electron-bombarded CCD or EBCCD). In this way, some gain is obtained and the electron image is accurately transferred to the CCD. However, the device does not yet exist as a commercially available x-ray camera. Visible light sensing devices do exist, Fig. 10, and the MTF performance is shown in Fig. 7. A scintillator deposit on this device would somewhat reduce this MTF performance but the final performance will have to measured once the device is assembled. The gain from such a device allows a higher frame rate between images to be used, or to use higher magnifications in spite of the reduced flux.

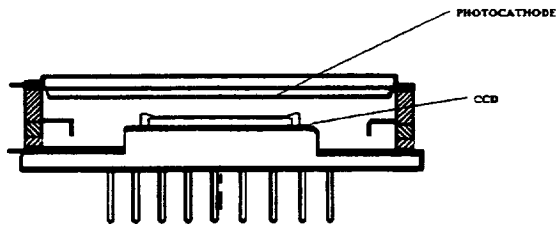

Figure 10. 512x512 pixel proximity focused electron-bombarded CCD cross-section low light level sensor manufactured in a cooperative research and development effort by Scientific Imaging Technologies, Inc. and Intevac EO Sensors. The CCD is a back-thinned SITe SI502AB and the photocathode is GaAs. Graphic courtesy of Pixel Vision Inc.

Other sensor configurations have been evaluated but have been found less worthwhile for XTM use as it is presently configured. If the x-ray energies employed for XTM were raised to 100 keV and higher (to MeV), then a fiberoptic faceplate made from glass scintillator material would be a prime candidate.[17,22] Scatter of the image is reduced by the fiberoptic structure and the absorption is determined by the thickness of the faceplate. Bonding the faceplate to a CCD directly can also give good results. Intensification of a scintillator screen image can be obtained using a microchannel plate proximity focused to the photocathode and an output phosphor. Small x-ray intensifiers (ICCD) like this are available but have seen limited commercial use because of their small size. This would otherwise not be a problem here, except these devices have high gain and high noise. They are however, superior devices compared to the large intensifier tube.

Detector / converter technologies selected for implementation in the XTM

Based on our evaluation we have chosen two x-ray sensor technologies and set the specifications for implementation into the XTM. The first selection was the scintillator/fiberoptic/CCD stack. The CCD has the largest number of pixels available (CCD 05-30 with 1242 x 1152 pixels) having a 500,000 electron well-depth. The readout electronics will permit as many as 16 bits (128,000) gray scale resolution per pixel and a 1 MHz clock rate at 14 bits per pixel. The selected CCD will have to be cooled to -30 °C and sealed in an air tight housing to obtain the optimum performance level. Digitization will be performed in the camera and the images stored and subsequently enhanced in the computer. The second selection, which does not exist commercially at this time, will employ the electron bombarded CCD technology where a proximity focused photocathode is illuminated by a scintillator. The cooled, back-illuminated CCD would have 25 μm wide pixels in a 1024 x 1024 array. The sensor will be quite compact at 40 mm in diameter. The front window of the vacuum tube would be a fiberoptic faceplate and support a GaAs photocathode which is suited to the green emission of the CsI scintillator. Both these technologies promise improved real-time imaging of solidifying metals in a device compact enough to be practical for implementation in a space laboratory furnace system.

CONCLUSIONS

1. X-ray transmission microscopy is shown to be capable of imaging the solidification of optically opaque metal alloys in real time with resolutions of up to 30 μm. The study of the detailed dynamics of solidification processes have included interfacial features and morphologies, cellular growth, the solute boundary layer in the liquid and the deformation of the interface from voids.

2. A redesigned furnace that permits solidification to occur within a few millimeters of the x-ray source both increases the magnification and enhances the image quality by increasing the feature dimensions to take advantage of the MTF properties of the imaging sensor.

3. CCD technologies that maintain a high MTF performance and offers sensitivity will permit the observation of smaller, lower contrast specimens and do so with a shorter exposure to reduce motion induced blur.

4. Two sensor designs were found that best offer the advantages from 3 above. One, the scintillator/fiberoptic faceplate/CCD stack produces high resolution images with a high dynamic range and good sensitivity in the x-ray energy range needed with metal specimens. The second device, the EBCCD, offers gain like an intensifier while maintaining a high MTF performance.

ACKNOWLEDGMENTS

This work has been supported by the NASA Microgravity Science and Applications Division under the Advanced Technology Program. We wish to acknowledge the State of Alabama for support of the proof of concept for the XTM development through the Center for Microgravity Materials Research (CMMR) at the University of Alabama in Huntsville.

REFERENCES

1. H. Huppert in *Handbook of Crystal Growth, Fundamentals Transport and Stability*, D.T.J. Hurle, ed., (North Holland, 1993) 743-783.

2. M. R. Howells, J. Kirz and D. Sayre; "X-ray Microscopy", Scientific American, 264, 88-94 (1991)

3. F. P. Chiaramonte, G. F. Danier, J. Gotti, E. S. Neumann, J. Johnston, and K. J. De Witt; AIAA Paper 92-0845, (AIAA 30th Aerospace Sciences Meeting, Reno NV, Jan. 6-9, 1992).

4. P. G. Barber, R. F. Berry, W. J. Debnam, A. L. Fripp, G. Woodell, and R. T. Simchick; Journal of Crystal Growth, 147 (1995) 83-90.

5. G. R. Chappleman; Journal of Materials Science, 17 (1982) 2208.

6. S. Rondot, J. Cazaux, O. Aaboubi, J. P. Chopart, and A. Oliver; Science, 263 (1994) 1739-1741.

7. E. W. J. Miller, and J. Beech; Metallography 5, 298-300 (1972)

8. M.R. Bridge, M.P. Stephenson, and J. Beech; Metals Technology, Nov. 1982, vol. 9, pg. 429

9. M. Kuriyama, R. C. Dobbyn, R. D. Spal, H. E. Burdette, and D. R. Black; J. Res. Natl. Inst. Stand. Technol. 95, (1990) 559-572

10. W. F Kaukler and D. O. Frazier; J Crystal Growth 71 (1985) 340 and NASA-TM 100317, Marshall Space Flight Center Dec. 1987.

11. K. A Jackson and J. D. Hunt; Acta Metallurgica 13 (1965) 1212.

12. R. Trivedi, J. A. Sekhar and V. Seetharaman; Met. Trans., 20A (1989) 769.

13. P. A. Curreri and W. F. Kaukler; "X-ray Transmission Microscopy Study of the Dynamics of Solid-Liquid Interfacial Breakdown During Metal Alloy Solidification", paper presented at the 8th International Symposium on Experimental Methods for Microgravity Materials Science, Feb. 4 Anaheim, Calif., 1996. Procedings to be published by The Metallurgical Society.

14. P. A. Curreri and W. F. Kaukler; "Real-time X-ray Transmission Microscopy of Solidifying Al-In Alloys ", Met. Trans., 27A (1996)

15. W. F. Kaukler and F. Rosenberger; "X-ray Microscopic Observations of Metal Solidification Dynamics", Met. Trans., 25A 1775(1994).

16. R. Clarke; Nuc. Instr. And Meth. In Phy. Res. A 347 (1994) 529-533.

17. I. T. Flint; *CCD X-ray Detection*, document prepared for EEV Ltd., Chelmsford Essex, England, Nov. 1991.

18. D. H. Lumb and J. A. Nousek; "Energy and Time Response of CCD X-Ray Detectors", IEEE Transactions on Nuclear Science, 39 n5 1379-1383(1992).

19. G. M. Williams Jr., A. L. Reinheimer, V. W. Aeibi, and K . A. Costello; "Electron Bombarded Back-Illuminated CCD Sensors for Low Light Level Imaging Applications",in *Charge-Coupled Devices and Solid State Optical Sensors V*, SPIE Vol. 2415, 1995.

20. J. C. Richard and M. Vittot; Nuc. Instr. And Meth. In Phy. Res. A315 (1992) 368-374

21. Thomson CSF X-ray tube manufacturer's specifications for 9 inch tri-field tube model TH 9428 HP, 1992.

22. Personal communications with representative from Princeton Instruments Inc., 1992.